Inter-band transitions in Zn_3P_2

1990 J. Phys.: Condens. Matter 2 2053

(http://iopscience.iop.org/0953-8984/2/8/012)

J. Phys.: Condens. Matter 2 (1990) 2053–2072. Printed in the UK

Inter-band transitions in Zn_3P_2

Jan Misiewicz
Institute of Physics, Technical University of Wrocław, Wybrzeże Wyspiańskiego 27, 50-370 Wrocław, Poland

Received 19 June 1989, in final form 6 September 1989

Abstract. Optical methods such as measurements of transmissivity, reflectivity and photoconductivity were used to investigate inter-band transitions in Zn_3P_2 at room temperature. The optical measurements were performed within the 1.4–5 eV energy range, for light polarised both parallel and perpendicular to the c axis of the crystal; with reflectivity, the measurements extended up to 11 eV, but for unpolarised light only. The birefringence of Zn_3P_2 crystal was also measured and was discussed in terms of band-to-band transitions. Transitions observed within the 4.5–11 eV energy range were interpreted on the basis of the pseudo-cubic energy-band structure model. However, this model could not be adopted to explain low-energy transitions. The band-structure model at the Γ point was suggested based on the results of measurements for polarised light and applying selection rules obtained from group-theory analysis. The direct energy gap of Zn_3P_2 at the Γ point was estimated in this model as 1.6 eV at 300 K, whereas crystal-field and spin–orbit splittings of the valence band were equal to 0.03 eV and 0.11 eV, respectively.

1. Introduction

Zinc phosphide (Zn_3P_2), always p-type semiconductor, has received growing attention in the last 10 years as a possible candidate for semiconductor devices. The main interest in this material is for solar energy conversion. The important factors necessary for the application of Zn_3P_2 in such devices are well fulfilled:

(i) Location of the optical absorption edge at 1.4–1.6 eV (Pawlikowski *et al* 1979, Fagen 1979, Misiewicz and Gaj 1981, Pawlikowski 1982), which is in the optimum range for solar energy conversion.

(ii) Minority-carrier diffusion length of about 10 μm (Nauka and Misiewicz 1981).

(iii) Both constituent elements are abundant and inexpensive.

There are a few papers devoted to the preparation and investigations of solar energy converters based on Zn_3P_2. A review of these studies has recently been made by Pawlikowski (1988). Thin Zn_3P_2 films were also used to produce ultraviolet detectors (Bendett and Hunsperger 1981). The distinct photodichroism observed on metal–Zn_3P_2 (oriented single-crystal) junctions was used as a light polarisation step indicator (Misiewicz *et al* 1984a).

Zn_3P_2 seems to be an interesting compound not only from the point of view of its possible applications but also because of its basic properties, especially band-structure parameters. However, they are still relatively unknown.

0953-8984/90/082053 + 20 $03.50

Experimental band-structure investigations are based mainly on the analysis of fundamental absorption and reflectivity spectra as well as on photoemission spectra. The fundamental absorption edge in Zn_3P_2 was measured in several works. Pawlikowski *et al* (1979) presented results of absorption measurements performed on single crystals in the range 1 cm^{-1} to 5×10^3 cm^{-1} and at 5, 80 and 300 K. Absorption on single crystals was also measured by Fagen (1979) in the range 1 cm^{-1} to 1.5×10^2 cm^{-1} at 300 K. The paper by Sobolev and Syrbu (1974) brought the absorption edge in the range of 3 cm^{-1} to 1.5×10^3 cm^{-1} but this curve is displaced almost parallel towards lower energies of about 90 meV. The absorption coefficient was measured on thin Zn_3P_2 films in a wide energy range (up to 2.3 eV) by Fagen (1979), up to $\alpha \simeq 7 \times 10^5$ cm^{-3} and by Żdanowicz *et al* (1980) in the energy range 1.55–2.0 eV. Absorption of Zn_3P_2 films was also measured in the 1.5–2.3 eV energy range by Murali *et al* (1986). Recently, the fundamental absorption edge was measured on oriented samples in polarised light in the absorption coefficient range 3 cm^{-1} to 6×10^2 cm^{-1} by Misiewicz and Gaj (1981) at 300 and 80 K.

Very preliminary reflectivity spectra of Zn_3P_2 in the 1.5–5 eV energy range were presented by Misiewicz *et al* (1980). Some data on reflectivity plots of Zn_3P_2 were also published by Sobolev and Syrbu (1974) and Fagen (1979). The results of reflectivity measurements in the 1.5–5 eV energy range performed on oriented single Zn_3P_2 crystals in polarised light were presented by Misiewicz *et al* (1984b). The valence band structure of Zn_3P_2 was investigated using photoemission techniques by Domashevskaya *et al* (1980). In that paper there are also some data on the conduction band structure.

The aim of this paper is to contribute to a better understanding of the band structure of Zn_3P_2. Band-to-band optical transitions are discussed using the results of wide-range spectral measurements of fundamental absorption, photoconductivity and reflectivity. The measurements were performed on oriented single crystals using polarised light within the 1.4–5 eV energy range. Reflectivity measurements were also extended to 5–11 eV energy range for unpolarised light. An additional source of information was measurement of birefringence.

The basis of the analysis of the experimental results has been the energy band structure of Zn_3P_2 calculated theoretically for the pseudo-cubic crystal structure by Lin-Chung (1971). The selection rules of the optical transitions obtained by us for polarised light determined on the basis of the group-theory analysis have also been taken into consideration.

2. Zn_3P_2 crystal structure

Zn_3P_2 is one of four crystallographically similar semiconductors of the $A_3^{II}B_2^{V}$ type, the others being Cd_3P_2, Zn_3As_2 and Cd_3As_2 (Żdanowicz and Żdanowicz 1975). The first two of them are strictly isostructural (Pistorius *et al* 1977) similar to the other ones. According to the papers by Stackelberg and Paulus (1935) and Pistorius *et al* (1977) the Zn_3P_2 lattice possesses tetragonal symmetry, belonging to space group D_{4h}^{15} ($P4/nmc$). The unit-cell dimensions are: $a = b = 8.0889 \times 10^{-10}$ m and $c = 11.4069 \times 10^{-10}$ m (Pistorius *et al* 1977), with eight formula units and 40 atoms. The crystal structure of Zn_3P_2 may be regarded as an Na_2O lattice to first approximation (or antifluoride lattice) in which one-quarter of the metal sites are vacant. As in the prototype antifluoride structure, cations and anions occupy alternate planes normal to the c axis. In this case, however, cation vacancies occur in pairs along all four body diagonals of the antifluoride subcell. The ordering of cation vacancies makes the volume of Zn_3P_2 unit cell four times

as large as the volume of the antifluoride subcell, and gives lower symmetry. Because of the vacancies, certain distortion can be found in the crystal structure. The Zn atoms are tetrahedrally coordinated with phosphorus atoms, being their nearest neighbours at the corners of a distorted tetrahedron. Every phosphorus atom is surrounded by zinc atoms located on six corners of a slightly distorted cube. The Zn_3P_2 crystal structure is schematically presented in figure 1(*a*), whereas figure 1(*b*) shows the basic defect antifluoride structure.

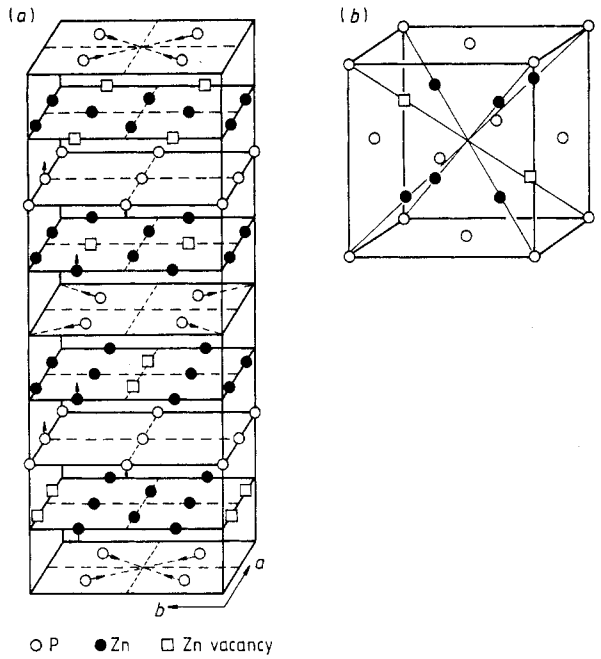

Figure 1. Zn_3P_2 crystal structure: (*a*) tetragonal unit cell; (*b*) basis defect antifluoride cell constructred from the tetragonal cell along the face diagonal of the base and the *c* axis. The *c*-axis vertical is elongated two times. Arrows denote atomic distortion directions (Steckelberg and Paulus 1935).

Zyubina *et al* (1977) reported high symmetry of O_h (m3m) for Zn_3P_2 crystal from extensive x-ray analysis. This result indicates that Zn_3P_2, although classified in the tetragonal structure, possesses a pseudo-cubic lattice with the reduced lattice parameter 11.45×10^{-10} m. This conclusion may be regarded as consistent with the previous discussion since the c/a ratio is approximately equal to $\sqrt{2}$ and, therefore, the cubic lattice, which contains eight defect antifluoride units, can be constructed from the tetragonal cell along the face diagonal of the base and the *c* axis.

3. Theoretical considerations

3.1 Bonding

The anion sublattice in Zn_3P_2 is nearly close-packed (FCC) as is visible in figure 1. This is a necessary condition for semiconducting properties (Mooser and Pearson 1961). The

bondings, however, are expected to be different for all compounds from II_3V_2 group in comparison with those of the III–V and II–VI groups. In contrast to the four valence electrons per atom for the III–V and II–VI compounds, there are only seven electrons for every two atoms for the II_3V_2 compounds. Compounds of III–V type normally have tetrahedral bonding with only four of the eight tetrahedral sites in the FCC structure occupied. For II_3V_2, six of the eight such sites are occupied. Such a structure, more tightly filled by the metal atoms, enhances the interaction between them and increases the metallic contribution to the bond. The smaller energy band gaps in II_3V_2 materials in comparison with those of III–V ones with the same anion is an example that more metallic contribution actually affects the physical properties.

The average number of valence electrons per bond is 4/3 rather than 2 electrons as it is in conventional tetrahedrally coordinated semiconductors. This relative deficiency of bonding electrons results in a distribution of equilibrium bond lengths. Figure 2 presents the distribution for all 96 bonds in the unit cell, calculated from the crystallographic coordinates given by Pistorius *et al* (1977) and sorted into 0.05×10^{-10} m wide bins. Most of the bond lengths (56) remain close to the sum of covalent radii in tetrahedral coordination (2.41×10^{-10} m). The remaining 40 bond lengths are placed in the range of $(2.6–2.8) \times 10^{-10}$ m, i.e. below the sum of ionic radii (2.86×10^{-10} m). The value of fractional ionicity of Zn_3P_2, $f_i = 0.19$, was determined from crystallographic data by an extension of Phillip's spectroscopic model, and $f_i = 0.17$ estimated from x-ray absorption edge shift by Adhyapak and Nigavekar (1978). The chemical bond for Zn_3P_2 is therefore a complex ionic–metallic–covalent bond.

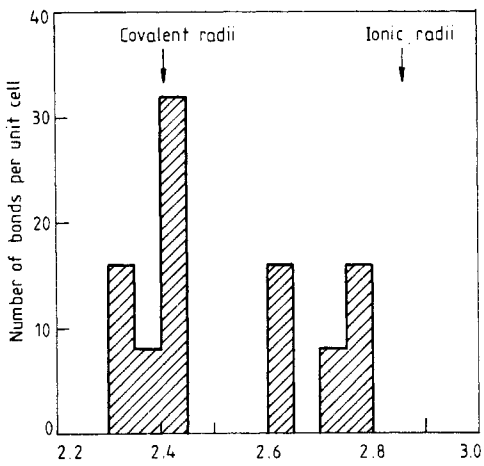

Figure 2. Distribution of bond lengths in unit cell of Zn_3P_2 calculated from crystallographic data given by Pistorius *et al* (1977), and rounded to the nearest 0.05×10^{-10} m.

3.2. Pseudo-cubic energy band structure model

The theoretical calculation of the energy band structure of Zn_3P_2 has been a difficult task because of the large number of atoms present in the tetragonal unit cell. Despite the complexities, Lin-Chung (1971) carried out a calculation by means of pseudopotential method. A pseudo-cubic, antifluoride-like crystal structure of Zn_3P_2 was taken into account by an effective vacancy potential superposed on the zinc atomic pseudopotential assumed in the ideal antifluoride structure. It should be mentioned that the calculations were based on O_h^5 symmetry, but spin–orbit and crystal-field interactions as well as the presence of d electrons of Zn were neglected. Those calculations showed a triply

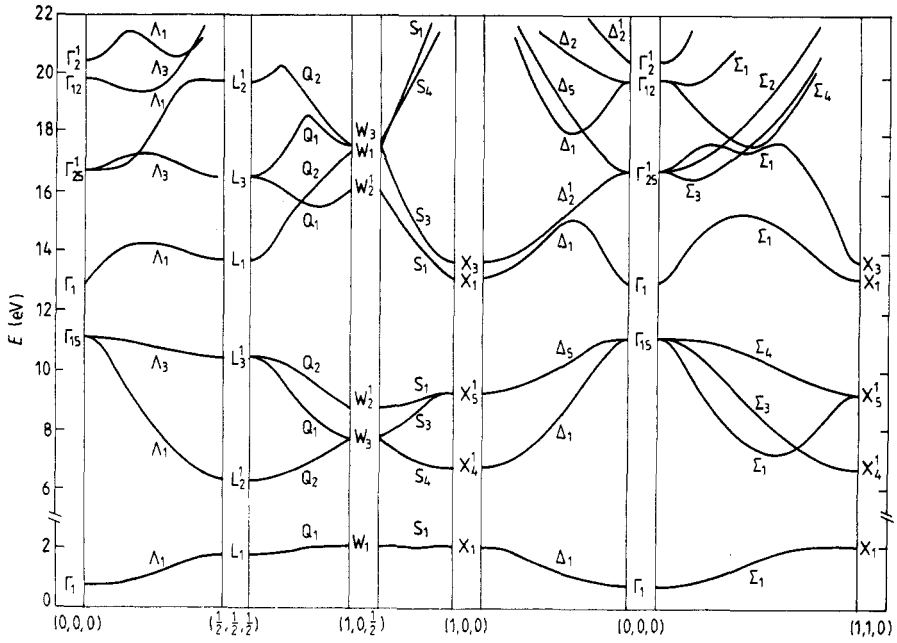

Figure 3. Energy band structure of Zn_3P_2 calculated in hypothetical crystal structure with O_h^5 symmetry by Lin-Chung (1971).

degenerate valence band maximum at the zone centre, and conduction band minima at the same point. The energy gap was determined as 1.89 eV.

The energy band structure obtained by Lin-Chung (1971) is presented in figure 3. According to the Lin-Chung calculations the lowest valence band is a phosphorus s-like level. The second band is a zinc s-like band. The third and fourth bands are s-like mainly zinc and p-like mainly phosphorus atoms.

The first Brillouin zone is shown in figure 4(*a*) for the hypothetical antifluoride crystal structure, for which the above calculations have been performed. Real symmetry analysis gives first Brillouin zone volume as only one-eighth of that of antifluoride structure and with completely different form (figure 4(*b*)). These notations of the points and axes are commonly used for O_h^5 and D_{4h}^{15} structure, respectively. Thus, we do not change the marking. To avoid ambiguity it will always be made clear which of the Brillouin zones is taken into account in further parts of the present paper.

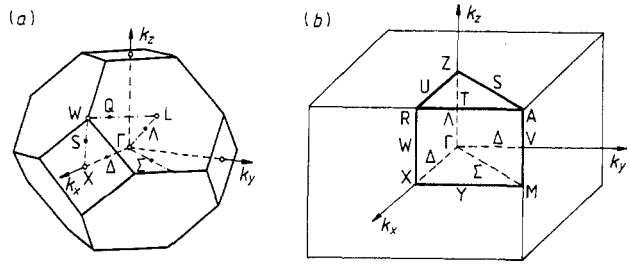

Figure 4. First Brillouin zone of Zn_3P_2 for (*a*) hypothetical antifluoride structure with O_h^5 symmetry and (*b*) real tetragonal structure with D_{4h}^{15} symmetry. Representation domains are indicated.

The problem is what changes can be expected on coming out of the Lin-Chung model to the band structure in the real crystal. A small potential, which is the difference between the potential used in the calculation and the potential of the real crystal, should be expected. Such potential should be small and it is rather difficult to evaluate it quantitatively. We can only state that its symmetry is D_{4h}^{15}. This potential will affect the electrons tending to mix states, which have wavenumbers differing from each other by the reciprocal-lattice vectors of the real structure. The potential will have its main influence on the states with small energy differences. The most important effect of its existence is mixing the states associated with Γ and X points in antifluoride structure. As a result, we expect the conduction band minima at the Γ point to be lowered and the valence band Γ_{15} to be raised, so the energy at the Γ point should be smaller than that calculated by Lin-Chung as 1.89 eV. Additional conduction band above Γ_1 coming out from the X_1 and/or X_3 states should occur (see figure 3). The residual potential and the spin–orbit interaction will lift the degeneracy of the maximum of the valence band Γ_{15}. When the potential acts, there will also be interactions between the valence level Γ_{15} and conduction band X_5', so the inter-band energy $X_5' \rightarrow X_1$ will increase. Similarly, the inter-band energy L_3'(valence band) $\rightarrow L_1$(conduction band) will decrease.

3.3. Spin–orbit and crystal-field effects

In order to obtain a reasonable model at the Γ point, theoretical considerations including spin and crystal-field effects connected with real tetragonal symmetry of the crystal are necessary. This indicated an analysis of the value of crystal-field splitting and spin–orbit splitting to be necessary.

At first, it is possible to estimate the spin–orbit splitting in simple antifluoride structure by means of the well known formula (see Cardona 1967)

$$\Delta_{so} = A[\lambda \Delta_{so}^{Zn} + (1 - \lambda)\Delta_{so}^{P}] \tag{1}$$

where λ is the ionicity of the compound, Δ_{so}^{Zn} and Δ_{so}^{P} are spin–orbit splitting values of free atoms. The constant A is very close to 1 for different semiconductors, so we have taken $A = 1$. Finally $\lambda = 0.18$ has been taken from Adhyapak and Nigavekar (1978). According to the small value of ionicity, correlated with the asymmetry in distribution of bonds, one can expect non-ionised or eventual singly ionised zinc and phosphorus atoms. Thus, we obtain $\Delta_{so} = 0.07$ eV for the former and 0.09 eV for the latter case. The last value is in a good agreement with the value of 0.11 eV calculated on the base of Lin-Chung model by Dowgiałło-Plenkiewicz and Plenkiewicz (1978). The latter paper also gives a value of crystal-field splitting as 0.03 eV. The same value was found by Cisowski (1982) from the lattice deformation analysis.

In the O_h^5 symmetry group, that of antifluoride cell, the levels of X, Y and Z symmetry transform according to the threefold degenerate Γ_{15} representation. In the D_{4h}^{15} group, the states of X and Y symmetry transform according to Γ_5^- representations and the states of Z symmetry according to the Γ_2^- representation. Owing to the spin–orbit interaction, the Γ_5^- state will split into a Γ_7^+ and Γ_7^- and the Γ_2^- state becomes Γ_7^-. Finally, because of the residual tetragonal potential and spin–orbit interaction, the threefold degenerate valence band maximum will be split into three levels Γ_7^-, Γ_7^+, Γ_7^-. The lowest conduction band in quasi-cubic Lin-Chung model Γ_1 will transform as Γ_6^+ in D_{4h}^{15} structure.

The order of the sub-bands can be determined experimentally, for example, by using the selection rules of the optical transitions.

3.4. Selection rules for direct optical transitions in real crystal structure of Zn_3P_2

Knowledge of the selection rules is necessary for interpretations of the optical measurements. First, in some cases band-to-band transitions can be forbidden. Furthermore, in the physical system, which has low symmetry, the selection rules can depend on the polarisation of light. In the case of the D_{4h}^{15} space group, the perturbation operator for direct optical transitions transforms as Γ_5^- for the light polarised perpendicular to the c axis and as Γ_2^- for light polarised parallel to the c axis. Thus, the selection rules for Zn_3P_2 depend on the polarisation direction of the light.

The first Brillouin zone of Zn_3P_2 real structure is presented in figure 4(b), with the points and lines of symmetry indicated.

By using the characters of the representation of the points and lines of symmetry as given in figure 4(b), the respective transition rules, taking into account the spin, may be obtained. Table 1 presents a list of the direct optical transitions allowed for both light polarisations. The common notation is used; see e.g. Olbrychski (1963) and Plenkiewicz and Dowgiałło-Plenkiewicz (1979).

Table 1. Direct optical transitions for Zn_3P_2 allowed both for $\boldsymbol{E} \perp \boldsymbol{c}$ and $\boldsymbol{E} \parallel \boldsymbol{c}$ light polarisations.

$\Gamma_i^{\pm} \rightarrow \Gamma_j^{\pm}$	$i, j = 6, 7$	
$Q_i \rightarrow Q_i$	$i = 6, 7$;	$Q = \Lambda, V$
$Q_5 \rightarrow Q_5$	$Q = Z, M, \Sigma, \Delta, U, W$	
$Q_i \rightarrow Q_j$	$i = 3, 5, i \neq j$;	$Q = \Delta\Sigma, US, X, R$
$Q_i \rightarrow Q_i$	$i = 3, 4$;	$Q = \Lambda\Delta, YW, \Lambda\Sigma$

Table 2 presents a list of the transitions that are permitted for $\boldsymbol{E} \perp \boldsymbol{c}$ polarisation. There are only a few transitions possible solely for $\boldsymbol{E} \parallel \boldsymbol{c}$ polarisation: $A_i^{\pm} \rightarrow A_i^{\mp}$, $i = 5, 6$, $Q_2^{\pm} \rightarrow Q_2^{\mp}$, $Q = T, S, Y$.

Table 2. Direct optical transition for Zn_3P_2 allowed only for the light polarisation $\boldsymbol{E} \perp \boldsymbol{c}$.

$\Gamma_i^{\pm} \rightarrow \Gamma_j^{\mp}$	$i, j = 6, 7$
$A_i^{\pm} \rightarrow A_i^{\pm}$	$i = 5, 6$
$A_i^{\pm} \rightarrow A_j^{\pm}$	$i, j = 5, 6$
$Q_i \rightarrow Q_i$	$i = 3, 4$; $Q = X, R, \Delta\Sigma, US$
$Q_i \rightarrow Q_j$	$i, j = 6, 7$; $Q = \Lambda, V$
$Q_i^{\pm} \rightarrow Q_i^{\pm}$	$i = 2, 3$; $Q = T, S, Y$
$Q_i \rightarrow Q_j$	$i = 3, 4$; $Q = \Lambda\Delta, YW, \Lambda\Sigma$

4. Sample preparation

Single-crystal growth was performed by using a chemical transport method, with iodine as active carrier, and directed vapour transport methods (for details see Misiewicz *et al* (1986) and Misiewicz and Królicki (1985)). By using the former technique, single crystals with dimensions of approximately $5 \times 3 \times 1$ mm^3 were obtained, whereas the other gave

single crystals approximately 0.9 cm diameter and 1–2 cm long. For the measurements, the samples were cut out from the boule with the appropriate thickness and mechanically polished using alumina powder with 1, 0.3 and 0.05 μm grain sizes. After polishing, the samples were degreased in acetone and methanol and then etched in 1.5–2% bromine methanol solution. For reflectivity measurements, we also used single crystals obtained by chemical transport growth with mirror-like as-grown surfaces. Absorption measurements were performed on the samples with different thicknesses from 5 mm to 10 μm. The thinnest samples were prepared by mechanical polishing up to 100–150 μm and finally by careful etching in bromine methanol solution. For photoconductivity measurements the samples were made with dimensions $8 \times 3\ mm^2$ and thicknesses within the range 100–300 μm. Electrical contacts were made on the extremities of the samples using gold chloride solution.

5. Results of measurements

5.1. Fundamental absorption edge

Absorption coefficient spectra were determined by means of transmission and reflectivity measurements in the 1.35–1.66 eV energy range. A standard Cary-14 system was used as well as equipment based on GDM-1000 monochromator, which is described extensively by Gumienny and Misiewicz (1982). The obtained absorption edge is presented in figure 5. In the 1.4–1.58 eV energy range a nearly exponential increase of absorption is found. Below 1.4 eV there is visible an absorption whose origin has not been determined unambiguously.

In the 1.58–1.62 eV range, the increase in absorption is changing to slightly slower, with a visible change in its slope at about 1.6 eV. In this figure are also presented absorption plots measured on thin films in the range 10^3–$2 \times 10^4\ cm^{-1}$ by Fagen (1979), in the range 4×10^3–$1.5 \times 10^4\ cm^{-1}$ by Żdanowicz *et al* (1980) and in the range 5×10^3–$2 \times 10^4\ cm^{-3}$ by Murali *et al* (1986). For thin film spectra, besides the change in slope at 1.6 eV there is another one visible at approximately 1.75 eV.

As Zn_3P_2 is a tetragonal material, it is necessary to perform the optical measurements using polarised light and oriented samples. For our measurements, the light was polarised by means of Carl Zeiss Jena polarisers with a polarisation grade better than 99%. Zn_3P_2 single crystals were oriented using a standard x-ray technique. Figure 6 presents absorption edges obtained for the light polarised parallel and perpendicular to the *c*-axis. For the absorption coefficient values smaller than $10^3\ cm^{-1}$ the lower-energy absorption plot is related to polarisation $\boldsymbol{E} \parallel \boldsymbol{c}$ whereas the higher-energy plot is related to $\boldsymbol{E} \perp \boldsymbol{c}$. The absorption plots cross at the energy of approximately 1.55 eV, for the absorption values of about $10^3\ cm^{-1}$. Such crossing was expected from the data published previously (Misiewicz and Gaj 1981, Misiewicz *et al* 1984a). Above the crossing the absorption plots for $\boldsymbol{E} \perp \boldsymbol{c}$ have the same slope at both lower and higher energies, whereas the absorption plot for $\boldsymbol{E} \parallel \boldsymbol{c}$ increases much slower above the crossing. The absorption plot for $\boldsymbol{E} \perp \boldsymbol{c}$ saturates above 1.6 eV where there is a point of distinct change in the slope. For $\boldsymbol{E} \parallel \boldsymbol{c}$ there is a small change in slope at 1.57–1.60 eV and a more prominent one at 1.62 eV. Absorption for $\boldsymbol{E} \perp \boldsymbol{c}$ in the range 1.58–1.62 eV is a few times stronger than for $\boldsymbol{E} \parallel \boldsymbol{c}$.

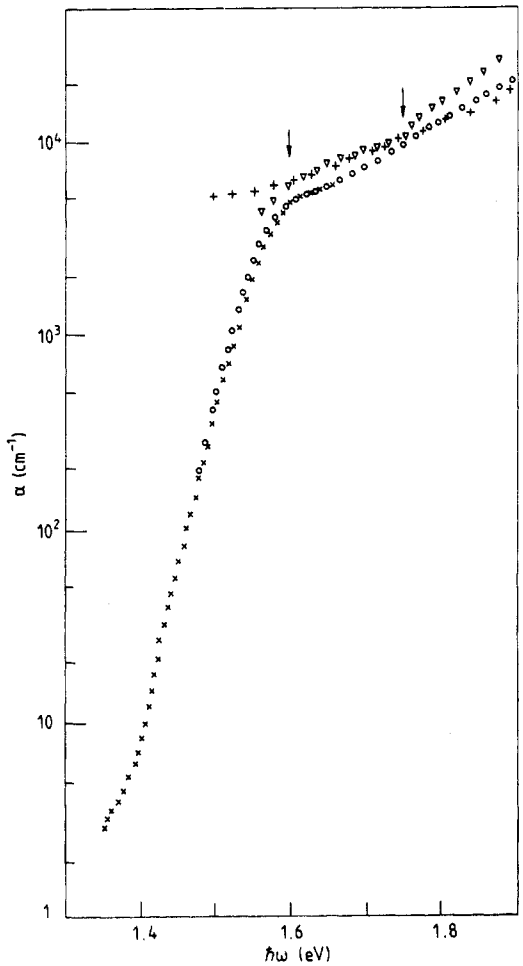

Figure 5. Fundamental absorption edge of Zn_3P_2 measured on single crystals. Data for thin films are also included. Arrows denote transition energies (see text and table 3). Symbols: ○, Fagen (1979); ∇, Żdanowicz *et al* (1980); +, Murali *et al* (1986); ×, this work.

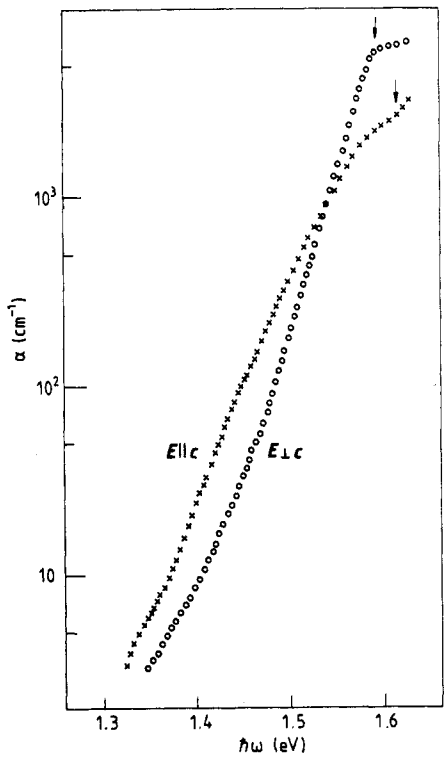

Figure 6. Fundamental absorption edge measured in polarised light on oriented single Zn_3P_2 crystals. Arrows denote direct energy gap value at appropriate polarisations.

5.2. Photoconductivity spectra

To perform photoconductivity measurements, standard experimental equipment was applied and described elsewhere (Misiewicz 1988). Figure 7 shows a representative plot of photoconductivity in the 1.45–2.7 eV energy range measured in unpolarised light. In this spectrum a few distinct singularities are visible at the energies 1.6–1.63, 1.74, 1.86, 2.07 and 2.55 eV.

Photoconductivity on the oriented samples was also measured, but in the 1.45–1.95 eV energy range only and using polarised light; see figure 8. Similarly to the absorption plot, two edges can be observed, one for $\boldsymbol{E} \parallel \boldsymbol{c}$ and the other for $\boldsymbol{E} \perp \boldsymbol{c}$. They cross at an energy of approximately 1.56 eV. Distinct changes in the slopes of

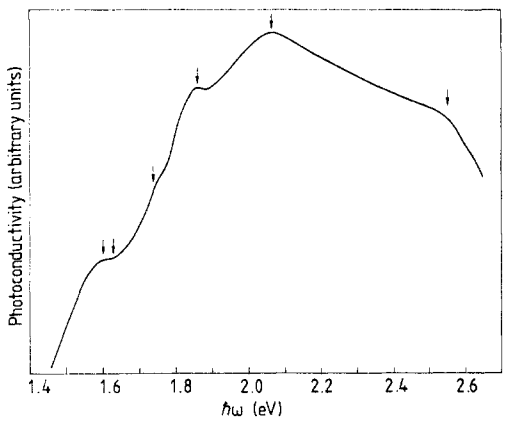

Figure 7. Photoconductivity spectrum of Zn_3P_2 in unpolarised light. Arrows indicate energies of band-to-band transitions.

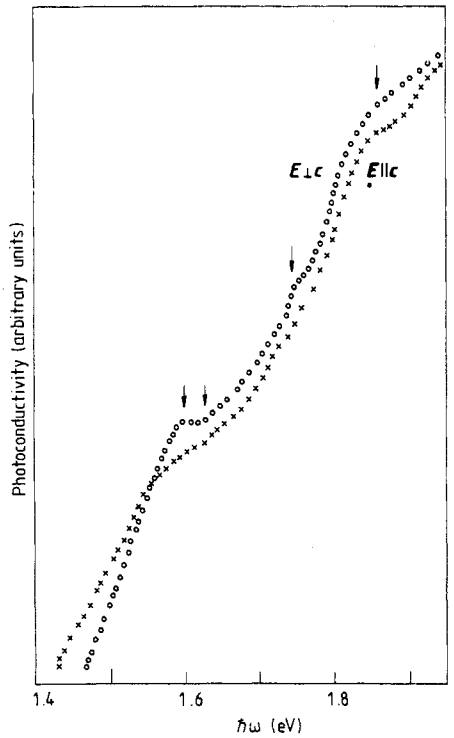

Figure 8. Photoconductivity spectrum of Zn_3P_2 at two different light polarisations. Arrows indicate energies of the transitions connected with the Γ point in the Brillouin zone (see also table 3).

photoconductivity curves are observed at 1.6 eV and at 1.63 eV for the $\boldsymbol{E} \perp \boldsymbol{c}$ configuration. In the same configuration there is also a step visible on the photoconductivity slope at 1.75 eV and a slight change of the slope in the 1.83–1.9 eV range. For $\boldsymbol{E} \parallel \boldsymbol{c}$, there are changes in the photoconductivity plot in the range of 1.55–1.65 eV and a more prominent change at 1.87 eV.

5.3. Reflectivity spectra

Reflectivity measurements were performed in two different set-ups. One was based on the SPM-2 and MDR-2 monochromators and allowed us to measure absolute value of reflectivity coefficient in the 1.3–6 eV energy range (for details see Becla *et al* 1979). In the 4–11 eV energy range, experimental equipment was based on a vacuum-ultraviolet MV-8 monochromator with a hydrogen discharge lamp (for details see Misiewicz *et al* 1989). In the 1.3–4.8 eV energy range, the measurements were also performed on oriented samples and for polarised light.

A typical fundamental reflectivity spectrum of Zn_3P_2 in the whole measurement energy range is presented in figure 9.

Figure 10 presents reflectivity plots obtained in polarised light. Both plots, obtained in different polarisations, are relatively similar. We observed two main transitions located at nearly the same energies for both polarisations. The maximum at 4.3 eV is

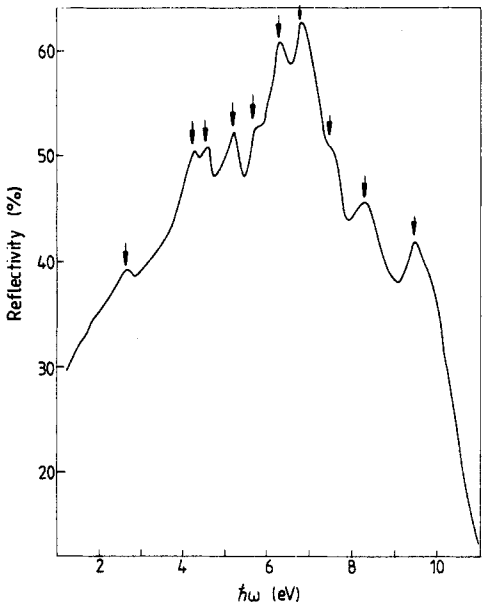

Figure 9. Reflectivity spectrum of Zn_3P_2 in unpolarised light.

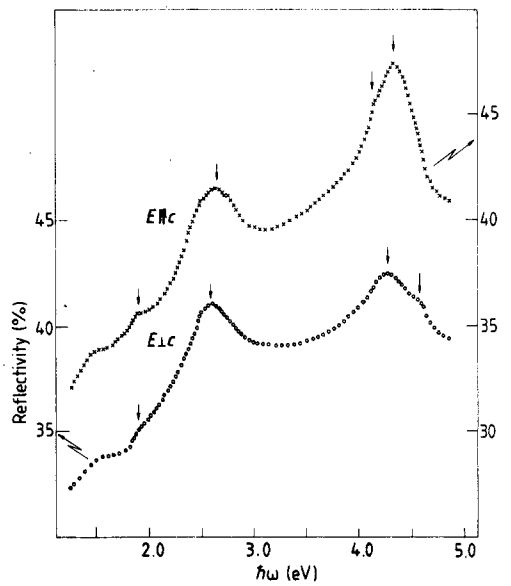

Figure 10. Reflectivity spectrum of Zn_3P_2 for two different light polarisations. Arrows denote the characteristic energies.

more promiment for $\boldsymbol{E} \parallel \boldsymbol{c}$ polarisation in comparison with the $\boldsymbol{E} \perp \boldsymbol{c}$ one. Transitions at 1.88 and 4.12 eV are more visible for $\boldsymbol{E} \parallel \boldsymbol{c}$, and the transition at 4.58 eV is stronger for $\boldsymbol{E} \perp \boldsymbol{c}$ polarisation. Figures 11(*a*)–(*c*) present the details of the plot within the 1.4–1.7 eV range (*a*) and the main maxima (*b*, *c*). For the $\boldsymbol{E} \perp \boldsymbol{c}$ polarisation, a small maximum is located at 1.59 eV and a change in slope of the reflectivity curve is visible at about 1.65 eV. A small minimum in the reflectivity plot is seen also at 1.63 eV for $\boldsymbol{E} \parallel \boldsymbol{c}$ polarisation.

5.4. Birefringence

In tetragonal crystals, there is a difference between refractive indices for light polarised parallel and perpendicular to the optical *c* axis. Zn_3P_2 birefringence was measured by two methods described extensively by Wardzyński (1970) and Gumienny and Misiewicz (1985). Figure 12 presents a typical plot measured within the 0.5–1.45 eV energy range. The birefringence spectrum is nearly energy-independent below 0.8 eV. For higher energies a distinct increase of birefringence value is visible. For Zn_3P_2 it was found that $n_\parallel > n_\perp$ (where $\parallel$ and $\perp$ mean $\boldsymbol{E} \parallel \boldsymbol{c}$ and $\boldsymbol{E} \perp \boldsymbol{c}$).

The birefringence

$$\delta n = n_\parallel - n_\perp \tag{2}$$

is connected with the dichroism, i.e. the difference between absorption coefficient for light polarised parallel and perpendicular to the *c* axis.

$$\delta \alpha = \alpha_\parallel - \alpha_\perp. \tag{3}$$

The measurement of birefringence is equivalent to determining the difference between the real parts of the dielectric constants, which are connected with the difference

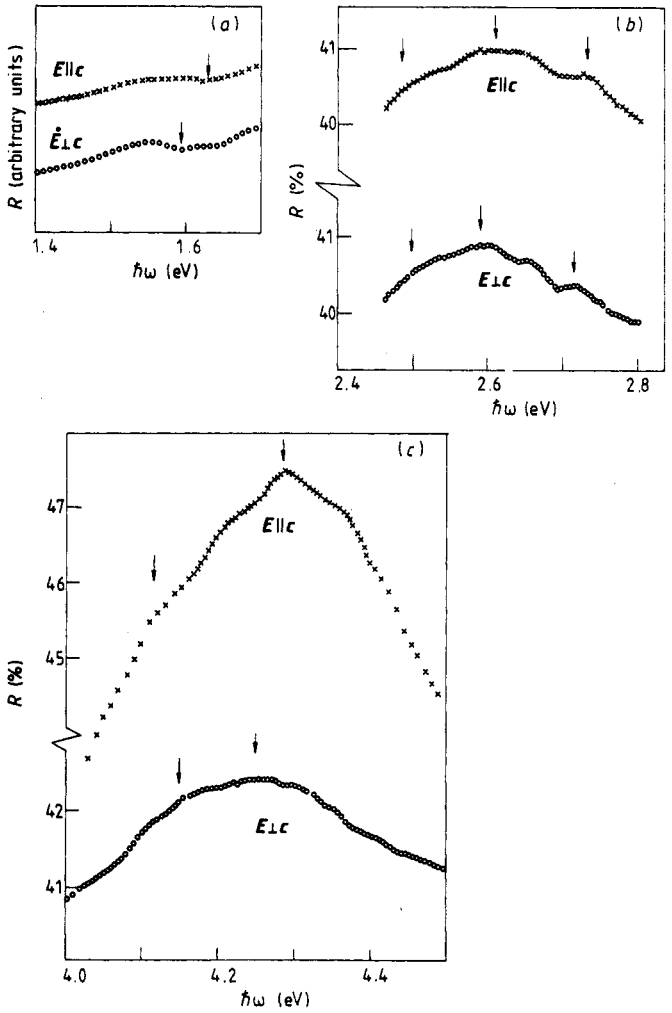

Figure 11. Details of the reflectivity spectrum in the three most important regions. Arrows denote the transition energies. The energy values are collected in table 3 for (*a*) and in table 5 for (*b*) and (*c*) cases.

of imaginary parts of dielectric constants, and further with dichroism. The Kramers–Kronig formula gives this relation (see Gaj 1973)

$$\delta n(E) = \frac{\hbar c}{\pi} \int_0^\infty \frac{\delta\alpha(x)}{x^2 - E^2}\,\mathrm{d}x \tag{4}$$

where E is photon energy, and $\hbar$ and c are universal constants.

By measuring the birefringence, we can obtain information about the dichroism plot in the photon energy range not attainable or very difficult to reach in transmission measurements. This makes it possible to analyse optical transitions at such energies.

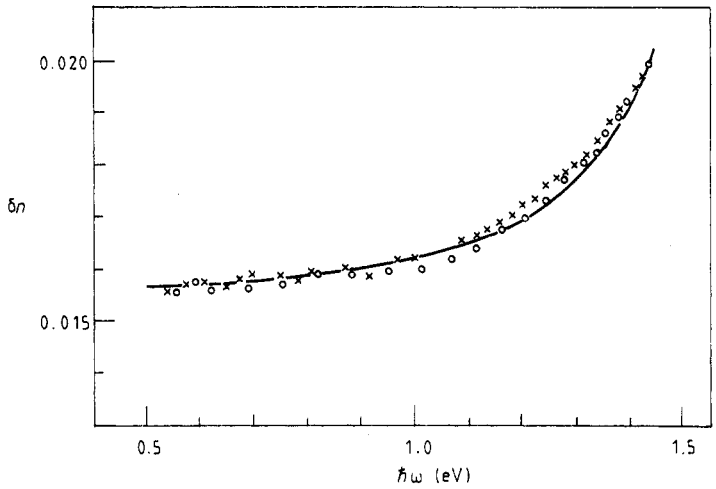

Figure 12. Birefringence dependence for Zn_3P_2 determined on two different samples marked by crosses and circles. The full curve is the theoretical model, with gap energy equal to 1.60 eV and minimised square standard deviation value.

From equation (4), assuming a delta-type function model of the dichroism, one obtains

$$\delta n(E) = \frac{\hbar c}{\pi} \frac{A}{E_0^2 - E^2} \tag{5}$$

where A is a fitting constant and E_0 is the characteristic energy.

By fitting the relation (5) to the experimentally obtained birefringence spectrum (see full curve in figure 12) one can determine the characteristic energy E_0. This energy usually corresponds to the smallest band-to-band distance (Gaj 1973). In the case of Zn_3P_2, $E_0 = 1.60$ eV is obtained at room temperature.

6. Discussion

6.1. Optical transitions at Γ point

The absorption is rising sharply within the 1.4–1.58 eV energy range. An exponential-like absorption increase is visible in this energy region.

The data from the absorption curve can be well fitted over almost three decades of the absorption range by the relation (Urbach 1953)

$$\alpha(\hbar\omega) = \alpha_0 \exp[-S(\hbar\omega_0 - \hbar\omega)] = \alpha_0' \exp(\hbar\omega/kT_0) \tag{6}$$

with $\alpha_0' \simeq 7 \times 10^{-22}$ cm^{-1} and $T_0 = 315$ K. The value of fitting constant T_0 is in relatively good agreement with the temperature of measurements, according to Urbach's original observations. The behaviour is commonly accounted for by the existence of a density-of-states tail and by optical transitions to such a tail of the conduction band (in the case of p-type material). In the Dow and Redfield (1972) model such an exponential absorption tail arises from exciton ionisation by localised internal electric fields, i.e. field-induced tunnelling of the photogenerated electrons away from the photogenerated

holes. The physical origin of these internal fields may result from phonons, impurities, dangling bonds, or any other sources of potential fluctuation.

In ionic crystals, it is common to correlate exponential behaviour of the absorption edge with the role of LO phonons in creation of active fields. In ordinary covalent semiconductors, the fields arise primarily from charged impurities. In view of the predominantly covalent character of the material the impurities are expected to be significant in field creation. Alternatively the internal fields may arise from the variation in bond lengths discussed in § 3.1, which constitute a form of localised elastic deformation not present in conventional tetrahedrally coordinated semiconductors (Dow 1972).

To determine the direct gap E_g from the absorption edge one can use the 'classic' dependence for absorption

$$\alpha\hbar\omega = A(\hbar\omega - E_g)^{1/2} \tag{7}$$

where A is a constant. By using this dependence a direct gap value of Zn_3P_2 at 300 K was determined on bulk samples as 1.51 eV (Pawlikowski *et al* 1979). By using the same formula (7) Żdanowicz *et al* (1980) found the energy of transition as 1.52 eV, and additionally transitions of 1.66 and 1.82 eV; Murali *et al* (1986) determined transition at the energy of 1.66 eV and next transitions at 1.75 and 1.82 eV. The analysis performed by Żdanowicz *et al* (1980) and Murali *et al* (1986) concerned thin-film absorption results only. Combining the results of measurements for bulk material and thin films, Fagen (1979) obtained a gap value of 1.55–1.60 eV and also next transitions at 1.9 and 2.05 eV. Pawlikowski (1982) fitted a three-band Kane-type model to the absorption plot combined from single-crystal and thin-film measurements, obtaining a set of transitions at 1.51, 1.55 and 1.72 eV.

In wide-gap semiconductors, the influence of excitons on the absorption is expected due to the Coulomb interaction of the electron and the hole produced in the transition process (Elliot 1957). Because of the small bonding energy of exciton ($\lesssim$10 meV) we can see excitonic peaks in absorption only at very low temperatures. At room temperature, owing to the exciton influence on band-to-band transitions, the energy gap is expected to be placed just above the exponential part of the absorption edge. The energy of abrupt bending of the absorption plot is very close to the energy gap of the semiconductor (see e.g. Sturge 1962).

Until now, in the case of Zn_3P_2, for energies higher than 1.55 eV the absorption results have been available only for thin films. The present paper gives absorption data on single crystals much more appropriate to analyse band-to-band transitions. As we can see in figure 5, the distinct change of absorption edge slope takes place at 1.60 eV ($\pm$0.02 eV). In the light of the discussion presented above, we may take this value as the energy gap value of Zn_3P_2 at room temperature.

Coming to the results for polarised light, absorption (see figure 6) and photoconductivity within the 1.4–1.65 eV energy range (see figure 8), transitions at 1.59 and 1.63 eV visible in both absorption and photoconductivity spectra correspond to weak features observed in reflectivity (see figure 11(*a*)). Such features in reflectivity are usually correlated with band-to-band transitions (Sell 1972).

Taking the Lin-Chung model as a basis for discussion we can find that transitions for energies not much higher than 2 eV should be connected only with the Γ point and its close neighbourhood. Making such assumptions and taking into account theoretical considerations from §§ 3.2–3.4, we may propose a band-structure diagram for the Γ point, shown in figure 13.

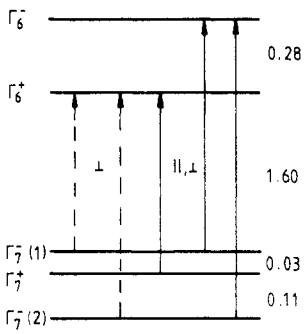

Figure 13. Model of the band structure of Zn_3P_2 at the Γ point determined on the basis of group-theory analysis for D_{4h}^{15} symmetry and experimental data. Energies in eV.

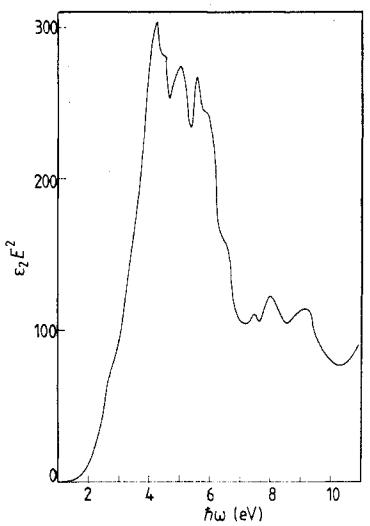

Figure 14. Quasi-joint density-of-states function for Zn_3P_2 calculated by means of Kramers–Kronig analysis of reflectivity spectrum presented in figure 9.

In table 3, a comparison is made of the experimental data obtained in the present and other works, concerning optical transitions in Zn_3P_2. Theoretical description of the observed transitions in terms of the model shown in figure 13 is also presented in table 3. The proposed model originates from group-theory considerations and is confirmed by observations of optical absorption and photoconductivity for polarised light.

On the basis of the above discussion, absorption and photoconductivity edges for $\boldsymbol{E} \perp \boldsymbol{c}$ correspond to $\Gamma_7^- \rightarrow \Gamma_6^+$ transition. The edge for $\boldsymbol{E} \parallel \boldsymbol{c}$ seems to be connected with $\Gamma_7^- \rightarrow \Gamma_6^+$ transition forbidden in dipole approximation as well as with $\Gamma_7^+ \rightarrow \Gamma_6^+$ transition allowed in both polarisations.

Table 3. Optical transitions in Zn_3P_2 within 1.5–2.1 eV energy range and their identifications by using group-theory analysis for D_{4h}^{15} symmetry (α, absorption; PC, photoconductivity; B, birefringence; R, reflectivity; ⊥, denotes $\boldsymbol{E} \perp \boldsymbol{c}$; ∥, denotes $\boldsymbol{E} \parallel \boldsymbol{c}$). The data from absorption measurements in other papers are included: F, data from Fagen (1979); M, data from Murali *et al* (1986); P, data from Pawlikowski (1982); Z, data from Zdanowicz *et al* (1980); energy in eV.

Description	Model energy	This work				Other sources			
		α	PC	B	R	F	M	P	Z
$\Gamma_7^-(1) \rightarrow \Gamma_6^+(\perp)$	1.60	1.59(⊥)	1.60(⊥)	1.60	1.59(⊥)	1.55–1.60		1.55	
$\Gamma_7^+ \rightarrow \Gamma_6^+(\perp, \parallel)$	1.63	1.62(⊥, ∥)	1.63(⊥, ∥)		1.63(∥)		1.66		1.66
$\Gamma_7^-(2) \rightarrow \Gamma_6^+(\perp)$	1.74		1.75(⊥)			1.77[a]	1.75	1.76	
$\Gamma_7^-(1) \rightarrow \Gamma_6^-(\perp, \parallel)$	1.88		1.86(⊥, ∥)		1.88(⊥, ∥)	1.9	1.82		1.82
$\Gamma_7^-(2) \rightarrow \Gamma_6^-(\perp, \parallel)$	2.02		2.07			2.05[a]			

[a] Visible as a change in absorption curve.

On the basis of the absorption, photoconductivity, birefringence and reflectivity measurements performed in polarised light, we can state that the direct energy gap in Zn_3P_2 is equal to 1.6 eV at 300 K. The same value of energy gap in Zn_3P_2 was proposed by Domashevskaya *et al* (1980) by using photoemission spectra, and Pawlikowski (1985) from absorption edge investigations of solid solutions of Cd_3P_2–Zn_3P_2. In photoemission investigations performed by Domashevskaya *et al* (1980) there was also a transition from valence band to conduction band at an energy of 2.2 eV. That transition seems to be correlated with the maximum observed by us in the photoconductivity spectrum at 2.07 eV.

The crystal-field splitting value $\Delta_{cf} = E(\Gamma_7^-(1)) - E(\Gamma_7^+) = 0.03$ eV and spin–orbit splitting value $\Delta_{so} = E(\Gamma_7^+) - E(\Gamma_7^-(2)) = 0.11$ eV, determined in this paper based on absorption, photoconductivity and reflectivity results, remain in very good accord with values obtained from other experiments as well as with those calculated theoretically by Dowgiałło-Plenkiewicz and Plenkiewicz (1978); see table 4.

Table 4. Energies of the crystal-field splitting Δ_{cf} and spin–orbit splitting Δ_{so} (α, absorption; PC, photoconductivity; R, reflectivity; C, Cardona relation (1)). The data from other papers are included: CJ, data from Cisowski (1982); P, data from Pawlikowski (1982); DP, data from Dowgiałło-Plenkiewicz and Plenkiewicz (1978).

	This work				Other sources		
	α	PC	R	C	CJ	DP	P
$\Delta_{cf} = E(\Gamma_7^-(1)) - E(\Gamma_7^+)$	0.03	0.03	0.04		0.03	0.03	0.04
$\Delta_{so} = E(\Gamma_7^+) - E(\Gamma_7^-(2))$		0.11		0.09	0.12	0.11	0.17

6.2. *Analysis of the high-energy transitions*

There is a row of optical transitions at energies higher than 2.2 eV, visible in the reflectivity spectrum. First, we will discuss results for polarised light. As can be seen in figures 10 and 11, the influence of crystal orientation on the reflectivity spectra for differently polarised light is rather small.

The band centred at 4.3 eV is more prominent for $\boldsymbol{E} \parallel \boldsymbol{c}$ polarisation in comparison with the $\boldsymbol{E} \perp \boldsymbol{c}$ case. The transition at 4.12 eV is more prominent for $\boldsymbol{E} \parallel \boldsymbol{c}$, but the transition for 4.58 eV is stronger for $\boldsymbol{E} \perp \boldsymbol{c}$. There are also small differences in the shape of the reflectivity curve and the energy position of singularities shown in figure 11. The energies of transitions observed in polarised light are listed in table 5. Furthermore, we can correlate the differences observed in the reflectivity plot with predictions of group-

Table 5. Singularities in the reflectivity spectrum of Zn_3P_2 for polarised light.

Type of light polarisation	Energy (eV)
$\boldsymbol{E} \parallel \boldsymbol{c}$	2.48, 2.62, 2.73, 4.12, 4.28
$\boldsymbol{E} \perp \boldsymbol{c}$	2.50, 2.60, 2.72, 4.15, 4.25, 4.58

theory analysis for the real D_{4h}^{15} structure of Zn_3P_2 crystal. The selection rules of the direct optical transitions allowed for different polarisations of light are presented in § 3.4. Group theory solves the problem of whether the matrix element of the appropriate transition is zero or not. The intensity of allowed transitions may be different due to different values of matrix elements. A large part of the tetragonal Brillouin zone is occupied by lines and points, where optical transitions are possible for both polarisations of light (see table 1). Thus it is comprehensible that most of the thresholds and maxima are visible on both plots in figure 10 for the same energies. As the reflectivity band at 4.3 eV is more prominent for $\boldsymbol{E} \parallel \boldsymbol{c}$, one can expect the existence of an additional factor of the transitions at lines T, S, Y and point A in the tetragonal Brillouin zone. The transition at 4.58 eV seems to be connected with one of the transitions allowed only for $\boldsymbol{E} \perp \boldsymbol{c}$ configuration, described in table 2.

It seems to be much easier to perform the interpretation of band-to-band transitions in terms of quasi-cubic Lin-Chung (1971) model. Such interpretation is valid because the anisotropy of reflectivity spectrum is small and, what is more important, a whole reflectivity spectrum is accessible only in unpolarised light.

The reflectivity spectrum of a semiconductor gives information on the energy distribution of the joint density of states (DOS). A more adequate representation of the DOS is given by the product of the imaginary part of the dielectric constant ε_2 and the square of energy (see Phillips 1966)

$$\text{DOS} \sim \varepsilon_2 E^2. \tag{8}$$

To obtain this relation from the reflectivity plot the well known Kramers–Kronig relations may be used. Applying appropriate approximations for reflectivity values below 1.3 eV and above 11 eV and using Kramers–Kronig relations one can obtain the relation (8) for Zn_3P_2 (see figure 14). The details of the approximation procedure as well as dielectric constant spectra ε_1, ε_2 for Zn_3P_2 are presented elsewhere (Misiewicz and Jezierski 1989).

From the dependence (8) (see figure 14), which reflects the DOS energy distribution, we can state that the main band-to-band optical transitions take place within 4–6 eV energy range with several local maxima (see also table 6).

Table 6. Energy (eV) of the singularities in reflectivity spectrum measured for unpolarised light and calculated optical function $\varepsilon_2 E^2$ for Zn_3P_2. The identifications are made on the basis of Lin-Chung (1971) theoretical band-structure model.

R	$\varepsilon_2 E^2$	Theory	Assignment	Symmetry
2.65	2.7	3.2	$L_3' \rightarrow L_1; \Lambda_3 \rightarrow \Lambda_1$	$M_0 (M_1)$
4.28	4.25	4	$X_5' \rightarrow X_1$	$M_1 + M_2$
4.60	4.55	4.4–4.7	$X_5' \rightarrow X_3; \Delta_5 \rightarrow \Delta_1, \Delta_2'$	M_3
5.25	5.05	5.3	$\Sigma_4 \rightarrow \Sigma_3$	$M_1 + M_2$
5.75	5.60	5.6	$\Gamma_{15} \rightarrow \Gamma_{25}$	$M_1 + M_2$
6.25	5.95	6.1	$\Gamma_3' \rightarrow L_3$	M_3
6.80	6.6	6.5–6.9	$\Lambda_3 \rightarrow \Lambda_3; X_4' \rightarrow X_1; \Delta_1 \rightarrow \Delta_1$	$M_3, M_1 + M_2$ (?)
7.50	7.45	7.3–7.5	$X_4' \rightarrow X_3; \Delta_1 \rightarrow \Delta_2'; W_2' \rightarrow W_2'$ (?)	$M_1 + M_2$
8.30	8.0	8.2–8.6	$\Lambda_3 \rightarrow \Lambda_3; \Gamma_{15} \rightarrow \Gamma_{12}; W_2' \rightarrow W_1, W_3; Q_2 \rightarrow Q_1, Q_2$	$M_1 + M_2$ (?)
9.50	9.15	9.3–9.4	$L_3' \rightarrow L_2'; \Gamma_{15} \rightarrow \Gamma_2'; \Sigma_1 \rightarrow \Sigma_4$	$M_1 + M_2$ (?)

It should be mentioned that the main band observed in the photoemission spectrum presented by Domashevskaya *et al* (1980) is also located within 4–6 eV, with sub-bands at 4.1 and 5.3 eV. It is not possible to see more details in that spectrum due to its qualitative and rather preliminary character. However, the general agreement between the result of Domashevskaya *et al* (1980) and the present paper is very good. In the same paper (Domashevskaya *et al* 1980) the position of the d level was found at 9.7 eV below the top of the valence band. That indicates that transitions correlated with the existence of the d level may occur near the energy 11.5 eV. The influence of d electrons on the band structure of Zn_3P_2 was neglected in the Lin-Chung (1971) model.

By using the Lin-Chung model presented in figure 3, and by applying standard analysis with the critical-point lineshapes method (M_0–M_3) (see Phillips 1966), we may correlate transitions possible in this model with the experimental data.

The first, relatively weak, transition located at 2.65 eV can be correlated with the $L_3' \rightarrow L_1$ process. Although the calculated energy of this transition is 3.2 eV, in the light of the discussion of residual tetragonal potential influence (see § 3.2) one can expect a considerable decrease of the energy. The peak at 4.3 eV can be connected with transitions at $X_5' \rightarrow X_1$, with energy of about 4 eV. In this case, the residual potential makes the calculated energy increase. Thus, we can say that general agreement between theoretical predictions and experimental results for these two transitions is very good. According to the discussion in § 3.2, we should expect much less influence of the residual potential on the band structure for higher band-to-band energy distances. Thus, the agreement between theory and experiment is expected to be better. The last statement seems to be confirmed by the results of a correlation procedure, which are presented in table 6.

7. Final conclusions

Optical and photoelectric methods were applied to investigate inter-band transitions in Zn_3P_2 at room temperature. Within the 1.4–1.9 eV energy range, the fundamental direct transitions were investigated by means of absorption, photoconductivity and reflectivity measurements performed on oriented samples for light polarised parallel and perpendicular to the *c* axis. From the results of these measurements the direct energy gap value was determined as 1.60 eV and the valence band was found to be split into three sub-bands with crystal-field splitting value equal to 0.03 eV and spin–orbit splitting value equal to 0.11 eV. The second conduction band was found at 0.28 eV above the lowest one. Theoretical analysis of birefringence measurements over a wide energy range also gave the value of fundamental optical transition of 1.60 eV.

Reflectivity was used within the 2–11 eV energy range as a tool of the experimental investigations up to energy of 5 eV, applying polarised light and further unpolarised light only. A good agreement between transitions observed in the 4.5–11 eV energy range and those predicted theoretically by quasi-cubic Lin-Chung (1971) band-structure calculations was found. To obtain a qualitative agreement between theory and experimental results, for the transitions at energies smaller than 4.5 eV it was necessary to take into account the influence of tetragonal perturbation potential on the bands of the Lin-Chung model.

In the model, any anisotropic properties were neglected, so the anisotropy in the reflectivity spectrum was discussed only in terms of group-theory analysis for the real tetragonal unit cell.

Complete disagreement between the Lin-Chung pseudo-cubic model and experimental results was found at the Γ point. A distinct anisotropy for the transitions within the 1.5–1.9 eV energy range was found. The analysis of the transitions possible at the Γ point performed in terms of the group-theory analysis for the real symmetry of Zn_3P_2 structure resulted in the order of the bands consistent with the experimental data.

Finally, we can say that short-range effects, for large k-vectors in Brillouin zone, seem to be influenced by tetragonal symmetry in the atomic ordering not as much as the long-range ones. It means that anisotropy of Zn_3P_2 crystal contributes more to the properties at the Γ point than beyond the Brillouin zone centre.

Acknowledgments

The author would like to express his appreciation to Dr P Becla from Francis Bitter National Magnet Laboratory, MIT, Cambridge, Mass., USA, who made it possible for him to perform photoconductivity measurements. The measurements of vacuum-ultraviolet reflectivity were performed at the Institute of Physics, Polish Academy of Sciences, Warszawa, Poland. It was possible due to the kindness and help of Drs B A Orłowski and B Kowalski from this Institute.

Helpful discussions with and critical reading of the manuscript by Professor J M Pawlikowski from the Institute of Physics, TUW, are deeply acknowledged.

This work was supported by the Polish Academy of Sciences under Contract CPBP 01.04.I.2.7.

References

Adhyapak S V and Nigavekar A S 1978 *J. Phys. Chem. Solids* **39** 171–3
Becla P, Gumienny Z and Misiewicz J 1979 *Opt. Appl.* **9** 143–50
Bendett M P and Hungsperger R G 1981 *J. Electron. Mater.* **10** 559–64
Cardona M 1967 *Semiconductors and Semimetals* vol. 3, ed. R K Willardson and A C Beer (New York: Academic) p 142
Cisowski J 1982 *Phys. Status Solidi* b **111** 289–93
Domashevskaya E P, Terekhov V A and Ugai Ya A 1980 *Proc. 1st Int. Symp. Physics and Chemistry of II–V Compounds, Mogilany, Poland* ed. M J Gelten and L Żdanowicz pp 225–35
Dow J D 1972 *Solid State Commun.* **4** 35–9
Dow J D and Redfield D 1972 *Phys. Rev.* B **5** 594–8
Dowgiałło-Plenkiewicz B and Plenkiewicz P 1978 *Phys. Status Solidi* b **87** 309–15
Elliot R J 1957 *Phys. Rev.* **108** 1384–9
Fagen E A 1979 *J. Appl. Phys.* **50** 6505–615
Gaj J A 1973 *Proc. 4th Conf. Physics of Semiconductors* (Warsaw: Institute of Physics, Polish Academy of Sciences) 39, pp 260–5
Gumienny Z and Misiewicz J 1982 *Opt. Appl.* **12** 37–47
—— 1985 *Opt. Appl.* **14** 63–8
Lin-Chung P J 1971 *Phys. Status Solidi* b **47** 33–9
Misiewicz J 1988 *Infrared Phys.* **28** 215–18
Misiewicz J and Gaj J A 1981 *Phys. Status Solidi* b **105** K23–5
Misiewicz J and Jezierski K 1989 *Solid State Commun.* **70** 465–9
Misiewicz J, Kowalski B and Orłowski B A 1989 *Acta Phys. Pol.* A **75** 67–73
Misiewicz J and Królicki F 1985 *Mater. Sci.* **11** 39–55
Misiewicz J, Królicki F, Lewicki M and Kasprzak J F 1986 *Acta Phys. Pol.* A **67** 1127–30
Misiewicz J, Mirowska N and Gumienny Z 1984a *Phys. Status Solidi* a **83** K51–6
Misiewicz J, Wrobel J and Jezierski K 1984b *J. Phys. C: Solid State Phys.* **17** 3091–9

Misiewicz J, Wrobel J, Sujak-Cyrul B and Królicki F 1980 *Opt. Appl.* **10** 75–8
Mooser E and Pearson W B 1961 *Prog. Semicond.* **5** 103–40
Murali K R, Gopalam B S V and Sobhanadri J 1986 *Thin Solid Films* **136** 275–80
Nauka K R and Misiewicz J 1981 *Phys. Status Solidi* a **65** K95–7
Olbrychski K 1963 *Phys. Status Solidi* **3** 214–49
Pawlikowski J M 1982 *Phys. Rev.* B **26** 4711–13
—— 1985 *J. Phys. C: Solid State Phys.* **18** 5605–16
—— 1988 *Rev. Solid State Sci.* **2** 581–602
Pawlikowski J M, Misiewicz J and Mirowska N 1979 *J. Phys. Chem. Solids* **40** 1027–33
Phillips J C 1966 *Solid State Phys.* **18** 55–164
Pistorius C W F T, Clark J B, Coetzner J, Kruger G J and Kunze O A 1977 *High Temp.–High Press.* **9** 471–82
Plenkiewicz P and Dowgiałło-Plenkiewicz B 1979 *Phys. Status Solidi* b **95** 29–37
Sell D D 1972 *Proc. Int. Conf. Physics of Semiconductors* (Warsawa: PWN) pp 800–6
Sobolev V V and Syrbu N N 1974 *Phys. Status Solidi* b **64** 423–9
Stackelberg M and Paulus R 1935 *Z. Phys. Chem.* B **24** 427–60
Sturge M D 1962 *Phys. Rev.* **127** 768–73
Urbach F 1953 *Phys. Rev.* **92** 1324–8
Wardzyński W 1970 *J. Phys. C: Solid State Phys.* **3** 1251–63
Żdanowicz L and Żdanowicz W 1975 *Ann. Rev. Mater. Sci.* **5** 301–27
Żdanowicz L, Żdanowicz W, Petelenz D and Kloc K 1980 *Acta Phys. Pol.* A **57** 159–65
Zyubina T A, Toropsev V P, Toropsev Yu P and Shchukin O 1977 *Izv. Akad. Nauk SSSR, Neorg. Mater.* **13** 335–7 (in Russian)